Journal of Applied Mechanics, Mechatronics and Energy System,
Vol. 1, Issue 1
October 2026
ISSN: XXXX-YYYY

Numerical Analysis of Flow and Combustion Characteristics in a Rotary Kiln with Varying dp/ds Ratios

Muhammad Ricky Ariza[1], Lohdy Diana[2*], Arrad Ghani Safitra[3]
[1] *Departement of Mechanical and Energy, ITS Raya Street, Surabaya 60111, Indonesia*
**Corresponding author: Lohdy Diana; Politeknik Elektronika Negeri Surabaya, Surabaya, Indonesia; email: lohdydiana@pens.ac.id*

Manuscript received July 04, 2026, revised September 03, 2026, accepted October 20, 2026
DOI: zz.yyyyy/xxxxx.pp134-1199

Abstract –*The combustion process inside rotary kilns plays a crucial role in determining flame stability, heat transfer, and temperature distribution. This study investigates the effect of the dp/ds ratio, defined as the ratio between the diameters of the primary and secondary air nozzles, on jet flame flow characteristics and temperature distribution in a rotary kiln using methane (CH_4) as fuel. Numerical simulations were conducted using Computational Fluid Dynamics (CFD) in ANSYS Fluent. The Realizable k–ε turbulence model, non-premixed combustion model with steady diffusion flamelet, and P-1 radiation model were employed to simulate turbulent combustion and radiative heat transfer. A two-dimensional axisymmetric domain was used with three dp/ds ratios of 0.044, 0.070, and 0.096. Model verification against reference data resulted in a Mean Absolute Percentage Error (MAPE) of 1.01%, indicating excellent agreement and reliability of the numerical approach. The results show that increasing the dp/ds ratio enhances fuel-air mixing, shifts the combustion zone closer to the burner inlet, and shortens the flame development region. The highest temperature of approximately 2600 K was obtained at dp/ds = 0.044, while increasing the dp/ds ratio to 0.096 reduced the peak temperature to approximately 2000 K due to enhanced air entrainment and lean combustion conditions.*

Keywords: *Rotary kiln, CFD, jet flame, dp/ds ratio, methane combustion, flow characteristics*
.

I. Introduction

Rotary kilns are widely used in industrial processes such as cement production, waste incineration, and metallurgical treatment because they can sustain continuous high-temperature operations. Their design and operating conditions influence heat transfer, product quality, and combustion performance [1], [2], [3]. Computational studies have also investigated heat transfer and radiative energy transport in systems involving granular materials, highlighting the importance of appropriate thermal modeling approaches [4]. Among the parameters affecting combustion behavior, burner geometry plays an important role in determining flame structure, flow distribution, and heat transfer within the kiln [2], [5].

One important geometric parameter is the ratio between the primary nozzle diameter dp and the secondary air diameter ds, expressed as dp/ds. Changes in burner geometry can affect the interaction between the fuel jet and surrounding air, thereby influencing the flow field, mixing behavior, recirculation zone, and flame length [6], [5], [7]. Studies of non-premixed, swirl-stabilized flames have also examined the relationship between flow-field characteristics and flame structure [8]. In addition, research on biomass pyrolysis in rotary kilns has shown that kiln geometry and particle-flow behavior can affect process conditions, although the mechanisms differ from gaseous-fuel combustion [9]. The air-to-fuel ratio is another important parameter affecting combustion behavior and numerical flow stability in rotary kilns [10].

Computational fluid dynamics (CFD) has been widely applied to investigate flow, combustion, and heat transfer phenomena in industrial kilns. CFD simulations provide detailed information on velocity fields, temperature distributions, and flame structures that are difficult to measure directly under high-temperature operating conditions. Previous studies have employed CFD to investigate rotary kiln burner performance [2], combustion dynamics in swirl-stabilized combustors [11],

and flame characteristics under non-premixed combustion conditions [12], [6], [7]. Other investigations have examined soot formation in turbulent non-premixed jet flames [13] and the flow and flame mechanisms associated with swirl-stabilized combustors [14]. CFD has also been used to analyze calcination and thermal behavior in rotary lime kilns [15]. In addition, studies on radiative heat transfer have highlighted the importance of selecting appropriate radiation models in numerical simulations [4], [16], [17]. Collectively, these studies provide a foundation for investigating the relationships between flow behavior, combustion characteristics, and heat transfer in industrial thermal systems.

Despite these investigations, the effects associated with varying the primary-to-secondary diameter ratio dp/ds require further examination for the burner configurations considered in this study. In particular, the relationship between changes in primary nozzle diameter, flow development, combustion-zone location, temperature distribution, and flame length needs to be assessed together. This study therefore investigates three dp/ds ratios, namely 0.044, 0.070, and 0.096, using a two-dimensional axisymmetric CFD model. The analysis focuses on velocity distribution, recirculation-zone development, temperature distribution, flame length, and combustion-species distribution. The simulations employ the Realizable k-epsilon turbulence model, the non-premixed probability density function (PDF) combustion model, and the P-1 radiation model [5], [17]. The results are used to compare the flow and combustion characteristics associated with the investigated burner configurations

II. Geometry and Methods

A. Geometrical Model

In In this study, a two-dimensional axisymmetric rotary kiln model was developed to investigate the effects of different burner diameter ratios dp/ds on flow and combustion characteristics. The computational domain represents an industrial rotary kiln comprising a burner inlet section, a cylindrical combustion chamber, and an outlet section [2], [3], [5].

The burner assembly consists of a central primary nozzle supplying methane (CH_4) and an annular passage for secondary air. Three dp/ds ratios (0.044, 0.070, and 0.096) were investigated by varying the primary nozzle diameter while maintaining the secondary diameter and the overall burner configuration as specified in the model. Changes in the primary nozzle diameter alter the inlet cross-sectional area and may consequently affect the primary-stream mass flow rate and momentum flux under the prescribed inlet conditions. The resulting flow-field and flame characteristics were therefore evaluated across the three geometric configurations [5], [10].

TABLE I.
GRID INDEPENDENCE STUDY

Mesh	Cells	Lf/do
A	1400	200
B	8866	169
C	16000	162
D	20000	156
E	25810	166

A structured quadrilateral mesh was generated throughout the computational domain. Local mesh refinement was applied near the burner exit and in regions expected to exhibit steep gradients in velocity, temperature, and species concentration. A grid-independence assessment was conducted using five meshes containing 1,400, 8,866, 16,000, 20,000, and 25,810 cells. The normalized flame length Lf/d0 was selected as the monitored parameter, where Lf is the flame length and d0 is the fuel nozzle diameter. The corresponding values were 200, 169, 162, 156, and 166, respectively, as summarized in Table I.

The relative changes in normalized flame length between successive meshes were 15.50%, 4.14%, 3.70%, and 6.41%, respectively. Although the change between Mesh B and Mesh C was relatively small, the increase from 156 for Mesh D to 166 for Mesh E indicates that the monitored parameter did not exhibit a consistent convergence trend. Therefore, the available results do not conclusively establish grid independence. Further mesh refinement and comparison of additional solution variables are required before the selected mesh can be considered independent of grid resolution.

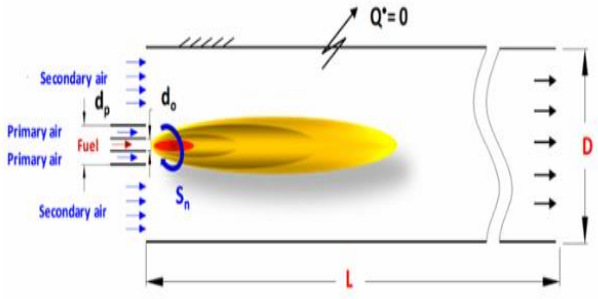


Fig. 1. Schematic of a 2D axisymmetric simulation domain representing the geometry of a rotary kiln

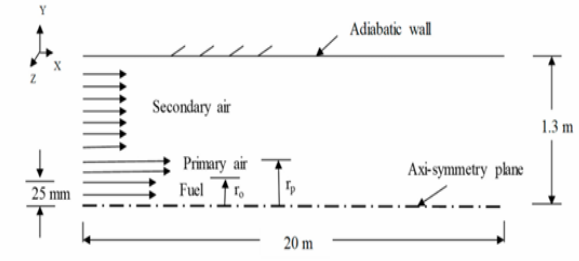


Fig. 2. Types of boundary conditions applied to axisymmetric 2D simulation domain

TABLE II.
SIMULATION PARAMETERS USED IN THE CFD MODEL

Parameters	Value	Description
Fuel	CH_4	Methane (gas)
Turbulence Model	Realizable k-ε	RANS
Combustion Model	Non-premixed PDF	Species transport
Radiation Model	P-1 Radiation	Heat transfer
Domain Dimension	2D axisymmetric	Kiln burner
Air Temperature	20 °C	Primary & secondary
Fuel Velocity	30 m/s	Reference journal
Fuel Temperature	20 °C	CH_4 Inlet

The three simulation cases were configured by varying the primary nozzle diameter dp while maintaining the secondary diameter ds at the value reported in Table III. The resulting dp/ds ratios were 0.044, 0.070, and 0.096. Since the primary inlet velocity was specified as 30 m/s in Table II changing the primary nozzle diameter also changes its inlet cross-sectional area. Consequently, the primary-stream mass flow rate and axial momentum flux may vary between cases, depending on the inlet density and the applied boundary conditions. Therefore, the observed differences in temperature distribution, flame length, and velocity field are interpreted as the combined effects associated with the change in primary nozzle geometry and its resulting flow conditions, rather than being attributed exclusively to the diameter ratio.

TABLE III.
SIMULATION CASES

Simulation	dp (m)	ds (m)	Ratio dp/ds
Var 1	0.115	2.6	0.044
Var 2	0.1825	2.6	0.070
Var 3	0.25	2.6	0.096

B. Numerical Methods

The numerical simulation was performed using ANSYS Fluent. A pressure-based solver with steady-state formulation was selected. The main numerical procedures are as follows:

- Turbulence model: Realizable k–ε with enhanced near-wall treatment
- Combustion model: Non-premixed model using mixture fraction–PDF approach
- Radiation model: P-1 radiation
- Discretization scheme: Second-order upwind for momentum, energy, turbulence, and species equations
- Pressure–velocity coupling: SIMPLE algorithm
- Convergence criteria: Residuals < 10^{-5} and stabilization of monitored variables (e.g., axial temperature, centerline velocity).

C. Boundary Condition

The boundary conditions were defined according to the burner configuration and operating conditions of the combustion system. The primary inlet supplied methane (CH_4), while the secondary inlet supplied air. The primary fuel inlet velocity was set to 30 m/s, and the fuel and air inlet temperatures were maintained at 20 °C. The secondary-air inlet velocity was specified according to the operating conditions of each simulation case.

The outlet was defined as a pressure outlet. The kiln walls were treated as no-slip, adiabatic surfaces, while the centerline was assigned an axisymmetric boundary condition. The Realizable k-epsilon turbulence model was employed to represent turbulent flow in the computational domain. The non-premixed probability density function (PDF) combustion model was used to simulate fuel-air mixing and combustion, following approaches applied in previous numerical studies of gaseous-fuel flames and rotary kilns [5], [7]. Radiative heat transfer was modeled using the P-1 radiation model [17].

The fuel and oxidizer streams were defined according to the non-premixed combustion model implemented in ANSYS Fluent. The inlet mixture-fraction boundary conditions and turbulence parameters were specified according to the numerical setup. These settings were applied consistently across the three investigated dp/ds ratios to compare the resulting flow and combustion characteristics.

- Primary inlet: Methane–air mixture, velocity inlet
- Secondary air inlet: Air at specified velocity, dependent on dp/ds configuration
- Outlet: Pressure outlet at kiln exhaust
- Walls: No-slip and adiabatic assumptions
- Axis: Axisymmetric constraint

D. Model Validation

The The CFD model was evaluated by comparing the simulated centerline temperature profile with reference data from the literature [5]. Elattar et al. [5] investigated methane combustion in a rotary kiln using ANSYS Fluent and a non-premixed PDF combustion model, and compared their numerical results with experimental data to assess the model performance [5]. Temperature was selected as the validation parameter in the present study because it reflects the combined effects of fluid mixing, combustion reactions, and heat transfer. The comparison was performed along the axial direction using the normalized coordinate x/do. The simulated and reference temperature profiles showed similar trends, particularly in the main combustion region.

The agreement between the two temperature profiles was quantified using the Mean Absolute Percentage Error (MAPE), yielding a value of 1.005524%. This result indicates a small average percentage difference between the temperature data included in the comparison. However, the MAPE value alone does not establish the accuracy of all predicted flow and combustion

characteristics. The exact number and locations of the comparison points, as well as the degree of equivalence between the reference geometry and operating conditions, could not be established from the available validation records. Therefore, the validation result should be interpreted as evidence of agreement for the selected centerline temperature profile, rather than conclusive validation of the entire CFD model.

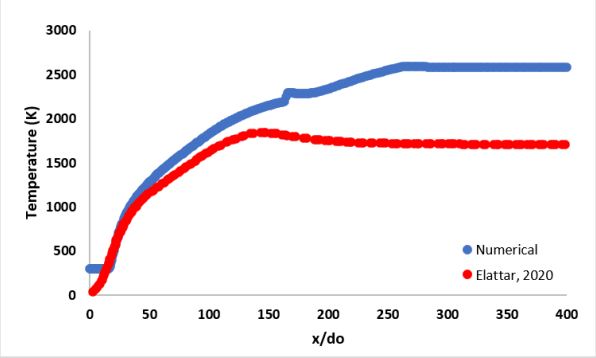


Fig. 3. Centerline temperature comparison

III. Result and Discussion

A. *Effect of dp/ds Ratio on Temperature Characteristics*

Figure 4 presents the temperature distribution contours for different dp/ds ratios. In general, all cases exhibit three main combustion regions, namely the initial mixing zone, the main combustion zone, and the downstream region. However, significant differences can be observed in the location of the high-temperature zone and flame development as the dp/ds ratio increases.

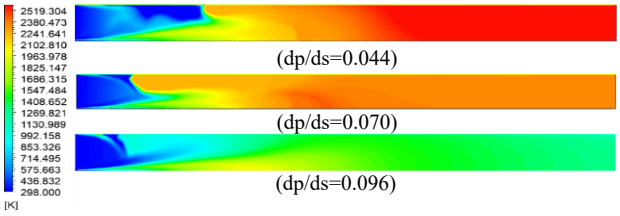


Fig. 4. Temperature distribution contours

For dp/ds = 0.044, the temperature increases gradually along the kiln axis, indicating a slower mixing process between methane and air. Consequently, the combustion zone develops farther downstream and produces a longer flame structure. The delayed heat release suggests that combustion is primarily controlled by the diffusion process between fuel and oxidizer.

Increasing the dp/ds ratio to 0.070 shifts the high-temperature region closer to the burner inlet. The flame becomes more compact, and the temperature rises more rapidly than in the previous case. This behavior indicates enhanced mixing intensity due to the increased momentum interaction between primary and secondary air streams.

At dp/ds = 0.096, the combustion zone forms closest to the inlet, indicating the fastest fuel-air mixing process. However, the peak temperature decreases compared with the other variations. This phenomenon suggests that although mixing is intensified, the larger amount of entrained air promotes lean combustion conditions, leading to thermal dilution and a reduction in maximum flame temperature.

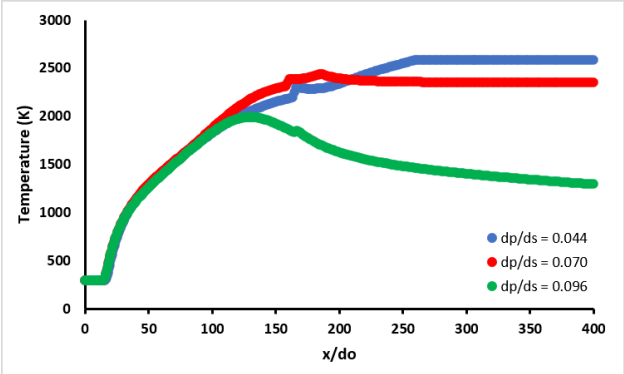


Fig. 5. Centerline temperature profiles for different dp/ds ratios

Figure 5 shows the centerline temperature profiles for different dp/ds ratios. All cases exhibit a similar trend in the near-burner region, where the temperature increases rapidly due to the initiation of fuel-air mixing and combustion. However, significant differences can be observed in the location and magnitude of the peak temperature as the dp/ds ratio increases.

For the dp/ds ratio of 0.044, the temperature increases gradually and reaches the highest peak temperature of approximately 2600 K at a relatively longer axial distance. The delayed temperature peak indicates a slower mixing process between methane and air, resulting in a longer combustion development region. As a consequence, heat release occurs over a larger portion of the kiln domain.

When the dp/ds ratio is increased to 0.070, the temperature rises more rapidly and reaches its peak closer to the burner inlet. The maximum temperature decreases slightly to approximately 2400 K, while the combustion zone becomes more compact. This behavior suggests that the higher momentum interaction between the primary and secondary air streams enhances fuel-air mixing and accelerates the combustion process.

A further increase in the dp/ds ratio to 0.096 causes the temperature peak to occur at the shortest axial distance. However, the maximum temperature decreases significantly to approximately 2000 K and subsequently declines along the downstream region. This phenomenon indicates that although the mixing process becomes more intensive, the larger amount of entrained air promotes lean combustion conditions, resulting in thermal dilution and a reduction in flame temperature.

Overall, increasing the dp/ds ratio shifts the combustion zone closer to the burner inlet and accelerates the combustion process. However, excessive increases in dp/ds reduce the peak temperature due to enhanced air

entrainment and leaner combustion conditions. Therefore, the dp/ds ratio influences not only the combustion location but also the thermal intensity and temperature distribution within the rotary kiln.

B. Effect of dp/ds Ratio on Flame Characteristics

Flame length was determined based on the centerline CH_4 mass fraction distribution. The flame termination point was defined as the location where the methane mass fraction approached zero, indicating nearly complete fuel consumption.

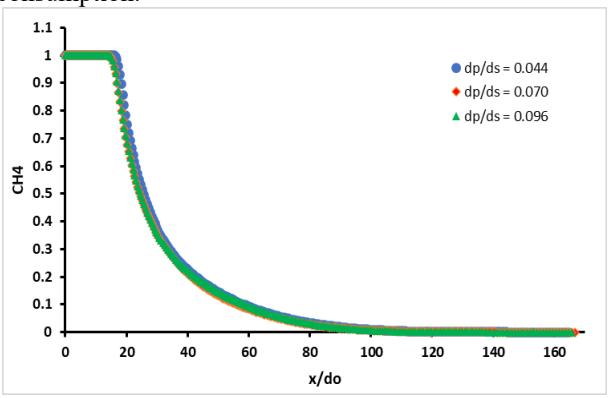


Fig. 6. Comparison of normalized flame length (L_f/d_o) for different dp/ds ratios

Figure 6 shows the CH_4 mass fraction profiles for different dp/ds ratios. In all cases, the methane mass fraction remains nearly constant near the burner inlet and then decreases rapidly as combustion progresses. The decrease in CH_4 concentration indicates fuel consumption through mixing and chemical reactions with the surrounding oxidizer.

The results show that increasing the dp/ds ratio accelerates methane consumption. For dp/ds = 0.096, the CH_4 mass fraction decreases more rapidly than the other variations, indicating that fuel-air mixing occurs more intensively. Consequently, the flame length becomes shorter because the fuel is consumed within a shorter axial distance. Conversely, the dp/ds ratio of 0.044 exhibits a slower reduction in methane concentration, resulting in a longer flame development region.

TABLE IV.
COMPARISON OF NORMALIZED FLAME LENGTH (L_f/D_o) FOR DIFFERENT DP/DS RATIOS

Variation	Lf (m)	Lf/do
dp/ds 0.044	8.22952	164.590
dp/ds 0.070	8.01818	160.364
dp/ds 0.096	7.96587	159.317

Table IV confirms that increasing the dp/ds ratio reduces the normalized flame length. The shortest flame was obtained at dp/ds = 0.096, whereas the longest flame occurred at dp/ds = 0.044. This result indicates that stronger fuel-air mixing promotes faster fuel consumption and earlier completion of the combustion process.

C. Effect of dp/ds Ratio on Flow Characteristics

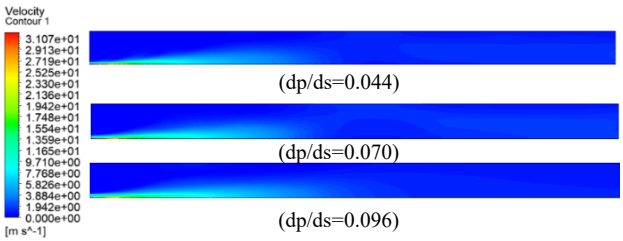


Fig. 7. Velocity magnitude contours

Figure 7 presents the velocity magnitude contours for different dp/ds ratios. In general, the high-velocity region is concentrated near the burner outlet and gradually decreases along the axial direction due to momentum dissipation and interaction with the surrounding fluid. However, noticeable differences can be observed in the penetration and distribution of the velocity field as the dp/ds ratio increases.

For dp/ds = 0.044, the high-velocity core is relatively narrow and decays rapidly downstream. The limited momentum interaction between the primary and secondary air streams results in a weaker entrainment process, causing the flow to spread gradually over a longer distance. Consequently, fuel-air mixing occurs more slowly, which is consistent with the longer flame structure and delayed temperature peak observed in Sections 4.1 and 4.2.

Increasing the dp/ds ratio to 0.070 enhances the momentum exchange between the air streams, resulting in a broader high-velocity region near the burner exit. The stronger entrainment promotes more intensive mixing and accelerates the combustion process. As a result, the combustion zone shifts closer to the inlet and the flame becomes more compact.

At dp/ds = 0.096, the velocity field extends further downstream and exhibits the widest momentum distribution among all cases. The stronger jet momentum increases the entrainment rate of surrounding air, leading to faster fuel-air mixing and earlier combustion initiation. This behavior explains the shorter flame length and upstream movement of the high-temperature zone observed in the previous sections.

Overall, increasing the dp/ds ratio enhances jet momentum and entrainment intensity, which improves mixing between fuel and oxidizer. The improved mixing accelerates combustion and shortens the flame development distance. Therefore, the flow characteristics play a significant role in determining flame behavior and temperature distribution within the rotary kiln.

Figure 8 presents the velocity vector and streamline distributions for different dp/ds ratios. The vector field illustrates the interaction between the primary jet and surrounding air within the rotary kiln, while the streamline

patterns reveal the formation of recirculation zones near the burner region. As the dp/ds ratio increases, the flow becomes more concentrated near the burner exit and exhibits stronger momentum transfer toward the downstream region.

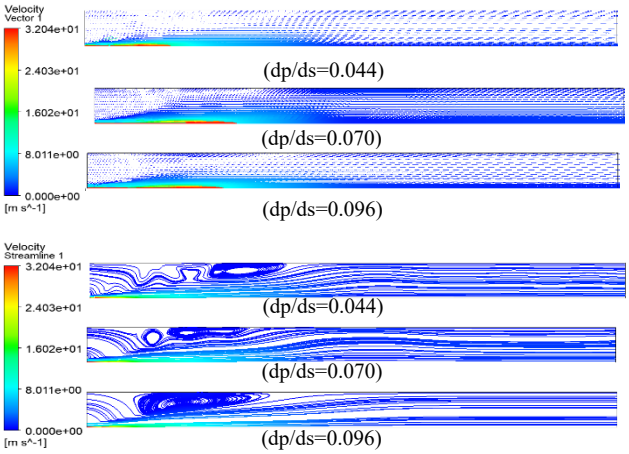


Fig. 8. Velocity vectors and streamline distributions for different dp/ds ratios

More pronounced recirculation structures can also be observed at higher dp/ds ratios, indicating enhanced entrainment and mixing between fuel and oxidizer. These recirculation zones contribute to flame stabilization by increasing the residence time of hot combustion products and promoting continuous ignition of incoming reactants. Consequently, the stronger mixing process accelerates combustion, shortens the flame length, and shifts the combustion zone closer to the burner inlet.

D. Effect of dp/ds Ratio on Combustion Species Distribution

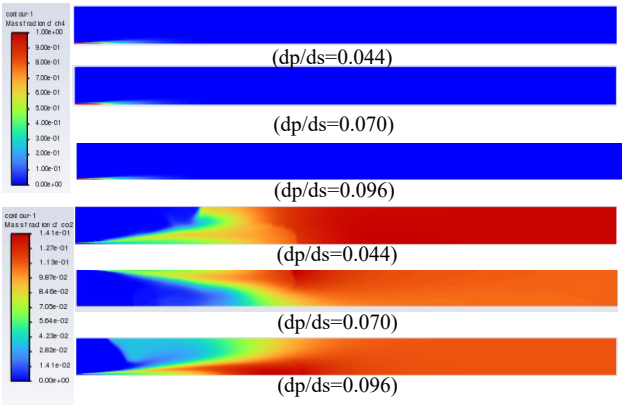


Fig. 9. CH_4 and CO_2 mass fraction distributions for different dp/ds ratios

Figure 9 presents the CH_4 and CO_2 mass fraction distributions for different dp/ds ratios. The CH_4 contours represent fuel consumption during the combustion process, whereas the CO_2 contours indicate the formation of combustion products. Together, these species distributions provide insight into the mixing characteristics and combustion completeness within the rotary kiln.

For all cases, the CH_4 concentration decreases along the axial direction as methane is consumed through oxidation reactions. However, the rate of methane depletion varies with the dp/ds ratio. At dp/ds = 0.044, the methane-rich region extends further downstream, indicating slower fuel-air mixing and a longer combustion development region. As the dp/ds ratio increases to 0.070 and 0.096, the CH_4 concentration decreases more rapidly near the burner outlet, suggesting enhanced entrainment of surrounding air and faster fuel consumption. This behavior is consistent with the shorter flame lengths and upstream movement of the combustion zone discussed in Sections 4.1 and 4.2.

In contrast, the CO_2 distributions exhibit an opposite trend. Since CO_2 is the primary product of methane combustion, its formation can be used as an indicator of combustion progress. For dp/ds = 0.044, significant CO_2 formation occurs further downstream, corresponding to the delayed combustion process observed in the temperature and flame analyses. As the dp/ds ratio increases, the CO_2 formation region shifts closer to the burner inlet, indicating earlier combustion initiation and more rapid oxidation of methane.

The species distributions confirm that increasing the dp/ds ratio enhances fuel-air mixing and accelerates the overall combustion process. Faster CH_4 depletion and earlier CO_2 formation demonstrate that higher dp/ds ratios promote more efficient reactant interaction. However, despite the accelerated combustion, the peak flame temperature decreases at higher dp/ds ratios due to increased air entrainment and lean combustion conditions. Overall, the species distributions support the trends observed in the temperature, flame, and flow analyses, confirming that the dp/ds ratio plays a significant role in controlling combustion behavior within the rotary kiln

TABLE V.
AIR MASS FLOW RATE AND AIR-TO-FUEL RATIO FOR EACH SIMULATION CASE

Parameter	Variation 1	Variation 2	Variation 3
dp/ds, based on AFR calculation	0.047	0.077	0.109
Primary air mass flow rate (kg/s)	0.15248	0.31795	0.53962
Secondary air mass flow rate (kg/s)	0.60113	0.59874	0.59553
Total air mass flow rate (kg/s)	0.75362	0.91669	1.13515
Methane mass flow rate (kg/s)	0.038388	0.038388	0.038388
AFR	19.63	23.88	29.57

The calculated air-to-fuel ratio (AFR) increased from 19.63 in Variation 1 to 23.88 in Variation 2 and 29.57 in Variation 3. This increase resulted from the higher total air mass flow rate while the methane mass flow rate remained constant at approximately 0.038388 kg/s. All

three AFR values exceeded the stoichiometric AFR of methane, approximately 17.2, indicating overall lean-mixture conditions. Variation 3 exhibited the highest AFR, corresponding to the largest air supply relative to the fuel flow rate. This condition may contribute to the lower maximum temperature observed in that case. However, the AFR represents the overall inlet mixture condition and does not independently describe the local mixture distribution inside the combustion chamber.

The relationship between AFR and flame characteristics should be considered together with the simulated temperature and species distributions. The increase in AFR across the three cases coincided with a decrease in maximum temperature. A higher overall air-to-fuel ratio can increase the dilution of the combustion products and influence the local heat-release distribution. Nevertheless, the temperature trend cannot be attributed to AFR alone because changing the primary nozzle diameter may also affect the inlet flow rate, jet momentum, and mixing behavior. Therefore, the results indicate an association between the changing air supply, burner geometry, and flame characteristics rather than an isolated effect of the dp/ds ratio.

IV. Conclusion

The effect of the dp/ds ratio on flow characteristics and jet flame performance in a rotary kiln has been numerically investigated using CFD. Based on the obtained results, the following conclusions can be drawn:

- The simulated centerline temperature profile showed good agreement with the reference data, yielding a Mean Absolute Percentage Error (MAPE) of 1.01%. This result indicates good agreement for the selected temperature profile but does not independently establish the accuracy of all predicted flow and combustion characteristics.
- Increasing the dp/ds ratio from 0.044 to 0.096 shifted the combustion zone closer to the burner inlet and accelerated the combustion process. However, the peak temperature decreased from approximately 2519 K to 1940 K due to enhanced air entrainment and lean combustion conditions.
- The velocity and species distributions showed changes in jet spreading and combustion development across the three cases. Increasing the dp/ds ratio was associated with broader radial flow distribution, earlier CH_4 consumption, and CO_2 formation closer to the burner inlet. These findings indicate changes in mixing and combustion behavior under the investigated geometric configurations.
- This study was limited to a two-dimensional axisymmetric, steady-state model, and the mechanical rotation of the rotary kiln was not explicitly represented. Future research should consider three-dimensional and transient simulations, including an appropriate representation of kiln rotation, to investigate flow and combustion phenomena beyond the scope of the present model.

Acknowledgements

This work was supported by Journal of Applied Mechanics, Mechatronics and Energy System (JAMMES).

References

[1] K. E. Peray and J. J. Waddell, The rotary cement kiln. Edward Arnold New York, NY, USA, 1986.

[2] D. M. Cecílio, M. Mateus, and A. I. Ferreiro, “Industrial Rotary Kiln Burner Performance with 3D CFD Modeling,” Fuels, vol. 4, no. 4, pp. 454–468, 2023, doi: 10.3390/fuels4040028.

[3] S. Yang, “Simulation research of a counter-flow rotary kiln hazardous waste incineration system,” Int. J. Coal Sci. Technol., vol. 9, 2022, doi: 10.1007/s40789-022-00523-y.

[4] J. Ma, C. Goniva, and S. Radl, “Particuology Predictions of the P1 approximation for radiative heat transfer in heterogeneous granular media,” vol. 82, 2023, doi: 10.1016/j.partic.2023.01.003.

[5] H. F. Elattar, E. Specht, A. Fouda, S. Rubaiee, A. Al-Zahrani, and S. A. Nada, “Swirled jet flame simulation and flow visualization inside rotary kiln-CFD with PDF approach,” Processes, vol. 8, no. 2, pp. 1–19, 2020, doi: 10.3390/pr8020159.

[6] R. D. Issafira, W. Wijayanti, L. Edahwati, W. D. Lestari, and W. Saputro, “Non-Premixed Combustion Simulation with Variation of Swirl Burner Slope using Turbulence Modeling K- ε,” vol. 1, no. 2, pp. 6–11, 2021.

[7] M. Hafid, N. Hebbir, M. Lacroix, and P. Joly, “CFD modelling of a turbulent CH4/H2/N2 jet diffusion flame with detailed chemistry,” Heat Mass Transf., vol. 59, no. 4, pp. 583–598, 2022, doi: 10.1007/s00231-022-03283-2.

[8] R. Palulli, S. Dybe, K. Zhang, and F. Güthe, “Characterisation of non-premixed, swirl-stabilised, wet hydrogen/air flame using large eddy simulation,” Fuel, vol. 350, p. 128710, 2023, doi: 10.1016/j.fuel.2023.128710.

[9] M. Pichler, B. Haddadi, C. Jordan, H. Norouzi, and M. Harasek, “Journal of Analytical and Applied Pyrolysis Influence of particle residence time distribution on the biomass pyrolysis in a rotary kiln,” J. Anal. Appl. Pyrolysis, vol. 158, no. April, p. 105171, 2021, doi: 10.1016/j.jaap.2021.105171.

[10] M. El Abbassi, D. Lahaye, and C. Vuik, “The effect of variable air–fuel ratio on thermal nox emissions and numerical flow stability in rotary kilns using non-premixed combustion,” Processes, vol. 9, no. 10, 2021, doi: 10.3390/pr9101723.

[11] M. Kapucu and J. B. W. Kok, “CFD-Based Prediction of Combustion Dynamics and Nonlinear Flame Transfer Functions for a Swirl-Stabilized High-Pressure Combustor,” Energies, vol. 16, no. 6, p. 2515, 2023, doi: 10.3390/en16062515.

[12] C. Yang et al., “Experimental Study on Flame Response Characteristics of a Non-Premixed Swirl Model Combustor,” Energies, vol. 16, no. 19, p. 6834, 2023, doi: 10.3390/en16196834.

[13] A. Kalbhor, D. Mira, A. Both, and J. Van Oijen, “LES investigation of soot formation in a turbulent non- premixed jet flame with sectional method and FGM chemistry,” no. 2024, 2025, doi: 10.1016/j.combustflame.2023.113128.

[14] P. Palies, “Flow and Flame Mechanisms for Swirl-Stabilized Combustors,” Aerospace, vol. 12, no. 5, p. 430, 2025, doi: 10.3390/aerospace12050430.

[15] J. Ryan and M. Bussmann, “CFD Modelling of Calcination in a Rotary Lime Kiln,” pp. 1–24, 2022.

[16] I. S. O. Barbosa, R. J. N. Santos, M. M. Dias, J. L. Faria, and C. G. Silva, “Radiation Models for Computational Fluid Dynamics Simulations of Photocatalytic Reactors,” Chem. Eng. Technol., vol. 46, no. 6, pp. 1059–1077, 2023, doi: 10.1002/ceat.202200551.

[17] H. F. Elattar, E. Specht, B. A. Almohammadi, M. H. Mohamed, and H. A. Refaey, “IMPACT OF P-1 RADIATION MODEL ON SIMULATED FREE JET FLAME CHARACTERISTICS OF GASEOUS FUELS The CFD with PDF Approach,” Therm. Sci., vol. 27, no. 5, pp. 3921–3938, 2023, doi: 10.2298/TSCI23010903E.